

Lecture 9: Solar Activity

Aims, learning outcomes, and overview

Aim: To describe magnetic reconnections, the array of solar activity, and the strong evidence that magnetic reconnection is the primary process involved in much solar activity.

Learning outcomes: At the end of this lecture, students are expected to:

- be able to explain qualitatively what is meant by magnetic reconnection;
- show using simple arguments the expected particle motions, outflow speed, and characteristic geometry for magnetic reconnection, including the differences between MHD and kinetic physics;
- appreciate and describe the qualitative features of magnetic reconnection models for solar flares;
- be aware of observational characteristics of solar flares, including gross energetics, classification, and some general features of flare X-ray and radio emission;
- be aware of the observational characteristics of CMEs, including gross energetics, and the connection between CMEs and flares;
- be able to describe the observational features of solar activity, including the sunspot cycle, the laws describing the patterns of polarity on the Sun as a function of the cycle, and the connections between the cycle, solar flares, and coronal mass ejections (CMEs);
- understand what is meant by magnetic helicity, and why it is of interest for solar flares and magnetic reconnection models.

Overview: *Solar activity* refers to transient solar phenomena associated with the Sun's magnetic field and in particular the 11-year cycle of that field. The most dramatic examples of solar activity are solar flares and CMEs, dynamic events in which magnetic energy is suddenly released in the solar corona. In this chapter an account is given of magnetic reconnection, examples of solar activity related to reconnection, and then a summary of observations and theories relating to flares and CMEs.

9.1 Magnetic reconnection

At its simplest level magnetic reconnection (or magnetic merging) involves two plasmas with frozen-in magnetic fields moving towards each other and converting the anti-parallel components of the magnetic field into rapidly moving, outflowing

plasma (enhanced directed kinetic energy) that has been heated (enhanced random kinetic energy). Such oppositely directed magnetic field components are standard at current sheets (e.g., helmet streamers in the corona and Earth’s magnetopause and magnetotail).

9.1.1 The MHD view of reconnection

Figure 9.1 illustrates the initial situation in the top panel, while then the characteristic result at a later time is in the bottom panel. The current sheet at the center of the figure is clear from taking the curl of \mathbf{B} , with \mathbf{J} pointing out of the page. (The systems is assumed to have infinite length into the page.) The central portion of this current sheet is called the “diffusion” region below, for reasons that will become apparent. Consider the left panel first in the limit $\mathbf{u} = 0$. Then the MHD induction equation

$$\frac{\partial \mathbf{B}}{\partial t} = \nabla \times (\mathbf{u} \times \mathbf{B}) + \frac{1}{\mu_0 \sigma} \nabla^2 \mathbf{B}, \quad (9.1)$$

has first term on the left hand side equal to zero. We are left with a standard diffusion equation whose physical solution is that the field diffuses towards the locations where it is small or zero, meaning towards the current sheet, and cancels out there by symmetry. Put another way, ohmic resistivity dissipates the currents responsible for spatial variations in the magnetic field. The energy in the magnetic field must then decrease with time and has to go somewhere, in this case into mechanical energy of the plasma itself. Consistent with this, we note that the current \mathbf{J} in the current sheet is parallel to the convection electric field \mathbf{E} , so that $\mathbf{J} \cdot \mathbf{E} > 0$ and work is done on the plasma (causing heating in the fluid picture).

Consider now the bottom panel of Figure 9.1 in the limit that $\mathbf{u} \neq 0$. In the diffusion region, where the spatial scales in Eq. (9.1) are small enough that the diffusion term dominates the convection term, the field lines are no longer convected with the fluid but instead are free to diffuse and to reconnect. Moreover, the incoming fluid cannot move across the center of the current sheet by symmetry, but instead must be squirted out parallel to the \mathbf{y} axis. The analogy is to fluid between two hands that are moving towards one another and the fluid squirts out in the plane of the hands. The incoming field lines are then broken and reconnected into outgoing field lines in the diffusion region. The diffusion region is said to have an “x-line” due to the shape of an X formed by the reconnected field lines. After reconnection the field lines are accelerated out the sides of the diffusion region by the magnetic tension force (which wants to straighten the field lines), which is assumed here to have finite extent in the y direction. The reason for assuming a finite extent is that the resistivity must be enhanced in the diffusion (reconnection) region if the reconnection is to occur on fast enough times to be of interest.

Some simple theory, along the lines of the Sweet-Parker theory, illustrates the basic features of reconnection. For energy release to occur, the outflowing plasma must have a weaker magnetic field. The energy has been converted into the bulk motion of the plasma, and so $\eta v_o^2/2 \approx B^2/(2\mu_0)$, where B is the magnitude of the field in the inflowing plasma, assumed to be much larger than that in the outgoing flow. This relationship implies that

$$v_o \approx B/(\mu_0 \eta)^{1/2} = V_A, \quad (9.2)$$

i.e. the plasma leaves the reconnection region at the Alfvén speed. This is an important prediction for observational testing.

In steady state Eq. 9.1 implies that $v_i B/l \approx B/(\mu_0 \sigma l^2)$, where l is a characteristic thickness for the diffusion region. Rewriting this, one finds that for MHD

$$l \approx \frac{1}{\mu_0 \sigma v_i}. \quad (9.3)$$

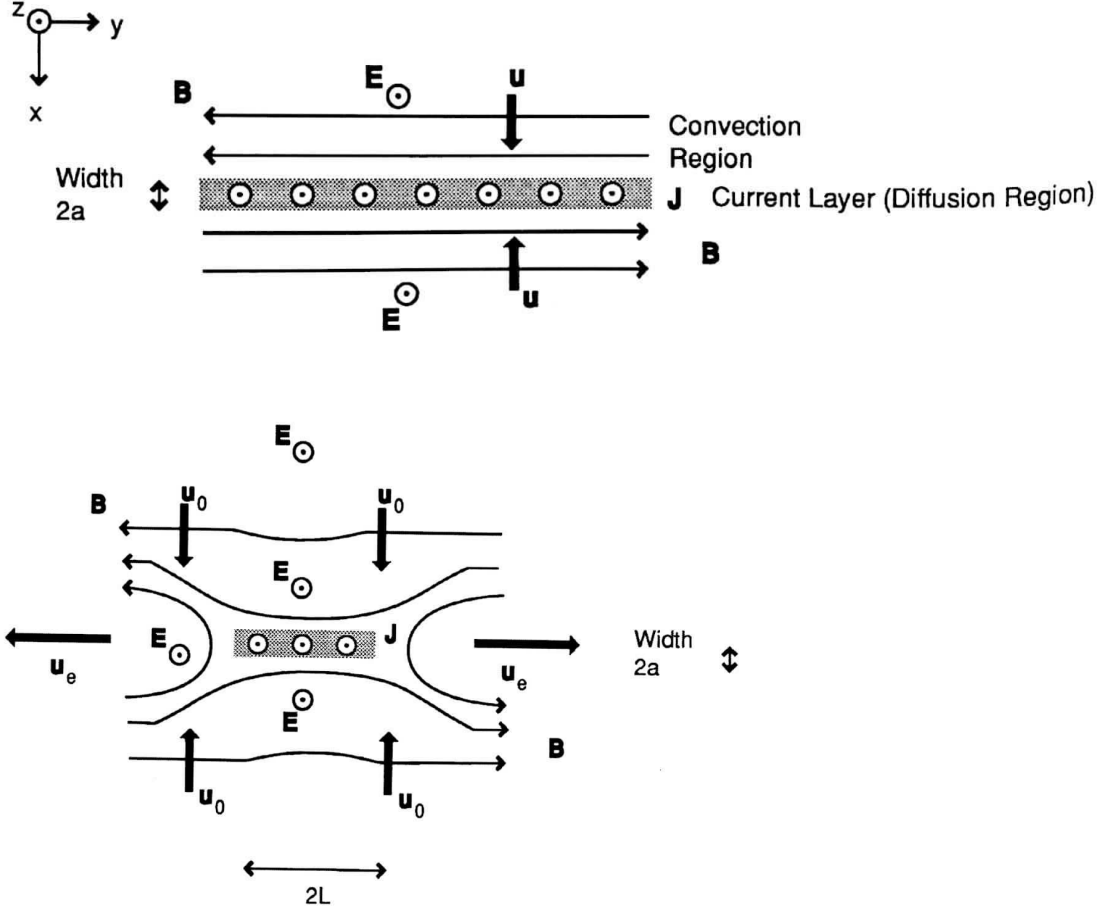


Figure 9.1: Schematics of magnetic reconnection [Cravens, 1997]. (Top) Initial condition for a current layer between impacting magnetized flows. (Bottom) Geometry of the reconnected flow and magnetic fields.

Conservation of mass requires that

$$v_i L \approx v_o l . \quad (9.4)$$

Accordingly the reconnection regions should be very thin, since typically one expects $v_i \ll v_o \approx V_A$.

Combining (9.2), (9.3) and (9.4) gives

$$v_i \approx \frac{v_A}{R_M^{1/2}}, \quad (9.5)$$

where

$$R_M = \frac{\mu_0 \sigma L^2}{L/V_A} = \mu_0 \sigma V_A L \quad (9.6)$$

is the magnetic Reynolds number. It is easy to see that $R_M = \tau_D / \tau_A$, where

$$\tau_D = \mu_0 \sigma L^2 \quad (9.7)$$

is the magnetic diffusion time and

$$\tau_A = L/V_A \tag{9.8}$$

is the Alfvén transit time for the length L . Hence R_M describes whether kinks in a magnetic field diffuse away or propagate away as Alfvén waves. If $R_M \gg 1$ then the diffusion time is long and magnetic perturbations are either convected away or propagate away as waves.

In the solar atmosphere, R_M is very large, and so the inflow speed is relatively small. The inflow speed is larger than the characteristic speed for diffusion ($v_D = L/\tau_d = v_A/R_M$), but it is still very slow, which is a problem because it limits the reconnection rate. So-called *fast reconnection* is required to explain the short timescales for energy release in flares. A more complex version of 2-D reconnection, the Petschek mechanism, achieves a somewhat faster rate.

A crucial development in reconnection theory was the recognition that current sheets may be unstable and allow multiple reconnection sites, a process known as the *tearing mode*. This process involves the current sheet breaking up into multiple “magnetic islands” or X-lines.

9.1.2 The kinetic view of reconnection

The kinetic physics of magnetic reconnection has been a very active field of research for the last 10 years, with major contributions by J. Drake, M. Hesse, and many others. No attempt is made to review this area now. Instead a few salient aspects are pointed out, in part to emphasize the importance of kinetic effects to explain the details of phenomena dimly viewed in the MHD picture and to emphasize the unknown aspects.

The very different gyroradii of electrons and ions suggest that their behaviour will differ inside the MHD diffusion region. Put another way, ions are expected to decouple from the magnetic field and behave in an essentially unmagnetized way when essentially a convected ion gyroradius ($= V_A/\Omega_{ci}$) from the center of the current sheet. However, electrons will remain magnetized and so tied to the magnetic field lines down to much smaller distances of order a convected electron gyroradius from the center of the current sheet. Figure 9.2 illustrates this situation [Zweibel and Yamada, 2009].

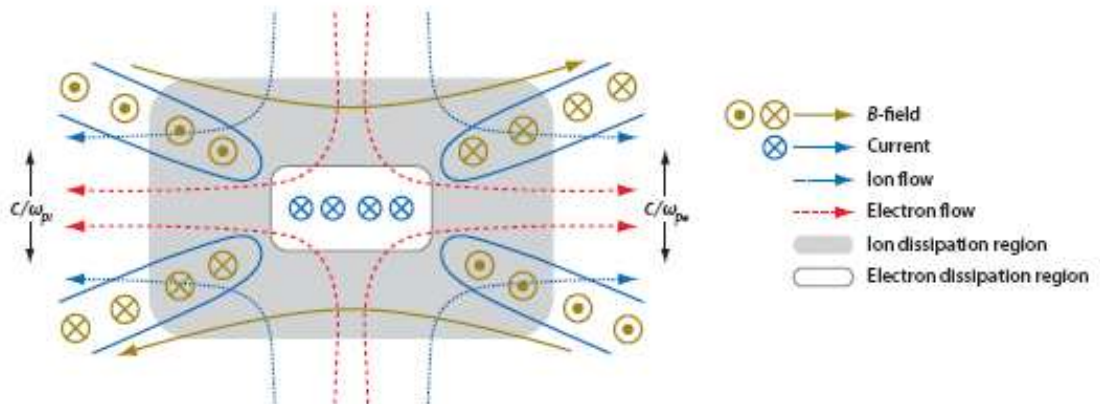


Figure 9.2: Kinetic view of magnetic reconnection [Zweibel and Yamada, 2009]. Electrons and ions decouple from the magnetic field in different regions, leading to currents and new behaviour.

The different motions of electrons and ions lead to currents and so magnetic fields (the so-called quadrupole magnetic field), as well as plasma waves that can heat and accelerate the particles. The waves are expected to be different in the electron diffusion and ion diffusion regions. Moreover, the $\mathbf{J} \times \mathbf{B}$ term in Ohm's Law, called the Hall term, becomes important at small spatial scales (since $\mathbf{J} \propto \nabla \times \mathbf{B}$).

Based on electrons and ions having different behaviour inside the reconnection region it can be expected that electrons and ions will be heated and accelerated differently. Figure 9.3 shows that this is the case for a reconnection event in Earth's magnetotail near the center of the plasmashet: the plasma shows fast flows near V_A in the v_x component away from the reconnection site, strong electron heating parallel to the magnetic field, and no evidence for ion acceleration or heating of either the electrons or ions [Oieroset et al., 2002].

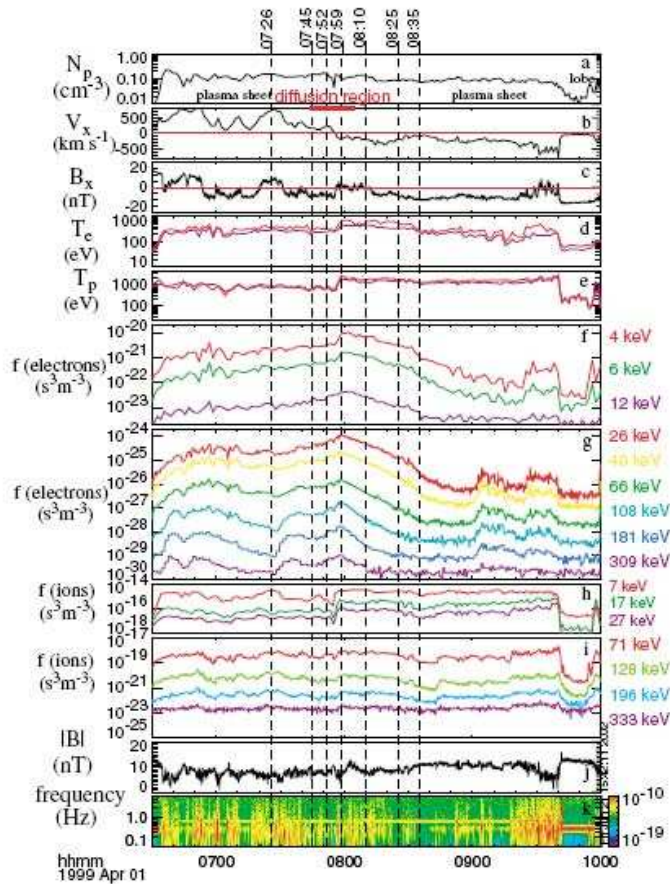


Figure 9.3: Wind spacecraft data for magnetic reconnection in Earth's deep magnetotail [Oieroset et al., 2002]. Note the fast flows in the v_x component away from the reconnection site, the strong evidence for electron acceleration parallel to \mathbf{B} , and minimal evidence for ion acceleration or heating. The wave data (bottom panel) are equivocal as to their relevance.

Most current research on reconnection involves 3D effects and considering the effects of multiple instabilities, such as the so-called "tearing modes" which split a current sheet like those in Figures 9.1 and 9.2 into multiple X-lines. Tearing gives rise to multiple reconnection sites and so multiple bursts of reconnection-associated activity (particle acceleration, flows, X-rays, radio waves etc.).

9.1.3 Simulations and observations of solar magnetic reconnection

Figure 9.4 shows resistive MHD simulations of a magnetic loop rising due to buoyancy into a pre-existing oblique magnetic field. (The resistivity increases when the current exceeds a threshold.) White lines show magnetic field lines, with clear evidence for reconnection. The reconnection outflows lead to a fast jet (left side) and to interactions with the denser plasma of the lower-lying loops on the right-hand side, leading to very hot loops there and associated X-rays. The X-rays can be produced as thermal emission from the hot plasma or as bremsstrahlung due to energetic particles slowing in a denser plasma.

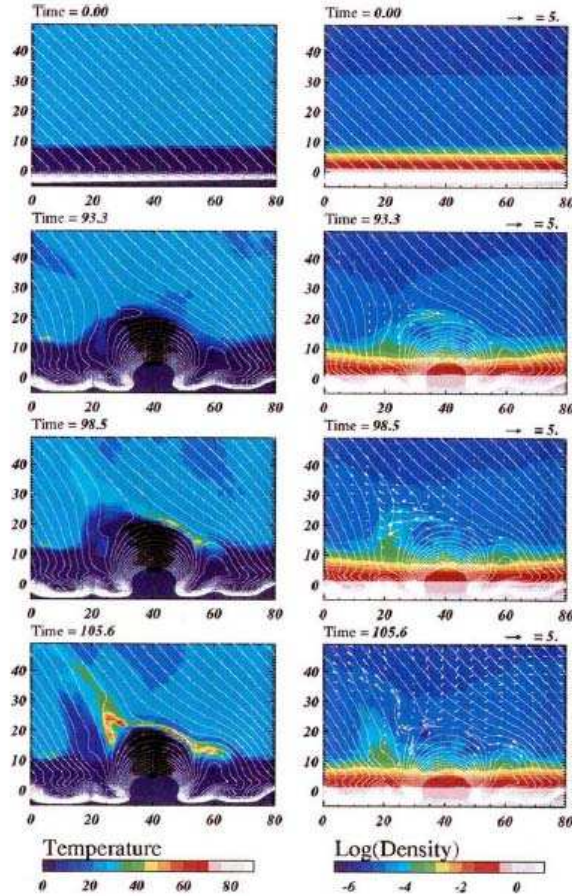


Figure 9.4: Resistive MHD simulation of reconnection in the solar atmosphere due to loops rising into an oblique coronal field [Yokoyama and Shibata, 1995]. (Left) Temperature and magnetic field as a function of time. (Right) Density, flow velocities, and magnetic field lines as function of time. Note the fast flows away from the reconnection site and the strong heating.

Figure 9.5 shows a buoyant loop rising into a horizontal field. The conversion of the overlying field into flow energy is clear.

Figure 9.6 illustrates the application of the two foregoing models of magnetic reconnection to solar X-ray events. Panels (a) and (c) show an “anemone X-ray jet” that appears strongly consistent with the model of Figure 9.4, while panels (b) and (d) show a “two-sided loop X-ray event” that appears strongly consistent with the model of Figure 9.5.

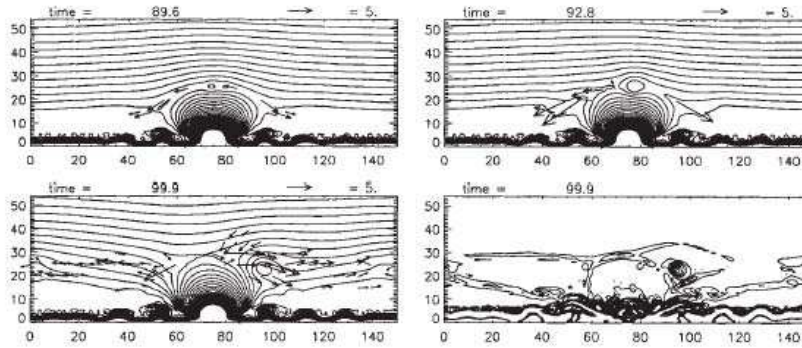


Figure 9.5: Resistive MHD simulation of reconnection in the solar atmosphere due to a loop rising into a horizontal coronal field [Yokoyama and Shibata, 1995]. Note the fast flows away from the reconnection site and the removal of the overlying coronal field.

9.2 Solar flares and CMEs

9.2.1 Flare theory

It is difficult to explain the rapid release of magnetic energy in flares because the diffusion timescale (9.7) is enormously long for values of the coronal conductivity and length scales typical of active regions. Two possible solutions to this problem are first that energy release occurs where the spatial scale for variation of the magnetic field is small, and second that the resistivity of coronal plasma may be enhanced by plasma instabilities. Both can be addressed in terms of magnetic reconnection.

There is a “standard model” for reconnection in flares involving reconnection occurring high in the corona. Figure 9.7 shows a variant of the standard model, due to Sturrock. Large arcade flares such as the ‘Bastille Day 2000’ flare, shown in Figure 9.8, are qualitatively consistent with this picture. This figure shows an image from the Transition Region and Coronal Explorer (TRACE) spacecraft of a region near the centre of the solar disk. The image is in inverse, so that the dark areas represent bright emission in the extreme ultraviolet. The large structure seen is an arcade of loops produced during the flare. The observed evolution of this structure is generally consistent with the model sketched in Figure 9.7. Reconnection is assumed to proceed at a topological structure (in 2-D, an X-point) above the observed arcade. In some gradual flares cusped soft X-ray loops are seen (e.g. Figure 9.9), suggesting a 2-D current sheet configuration above the loops. The scenario of Figure 9.7 also explains the spreading of $H\alpha$ ribbons in terms of reconnection at a rising X-point. Recent observations from the Yohkoh spacecraft also provide evidence that compact flares involve high-energy processes occurring outside the loop, and so the standard model has been claimed to apply to all flares. Weak points of the standard model include its failure to account for the energetic electrons responsible for flare emission, the problem that energy release is posited to occur in weak-field regions, and the fundamentally large-scale (rather than fragmentary) nature of the energy release.

The twisting, braiding, and helicity (a measure of the twist) of magnetic field lines become important in reconnection and flare theories because twisting leads to regions of local anti-parallel magnetic fields being created and moved towards each other. Accordingly, one can expect loops and field lines with significant helicity to be more likely to undergo a flare or reconnection event, with associated evolution of the magnetic field structure, release of energy, and movement of plasma.

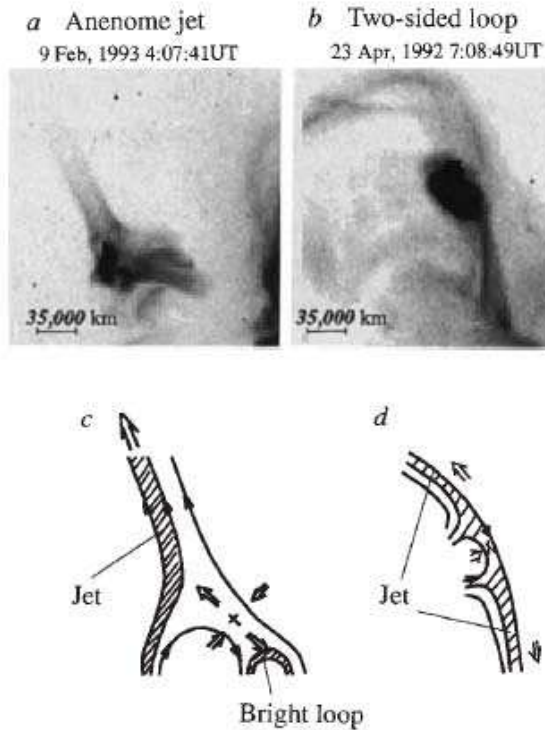


Figure 9.6: (a) Yohkoh spacecraft observations of an “anemone jet” in X-rays, (b) corresponding observations of a “two-sided loop” event, (c) the interpretation for part (a) based on Figure 9.4, and (d) the interpretation for part (b) based on Figure 9.5 [Yokoyama and Shibata, 1995]. The reconnection sites, fast flows, and X-ray jets are identified in (c) and (d).

9.2.2 Flare observations

Solar flares are dynamic events in which a large amount of energy ($10^{21} - 10^{26}$ J) is explosively released in the solar atmosphere on a short timescale ($10^2 - 10^3$ s). Originally flares were defined in terms of increased $H\alpha$ emission but now they are usually characterised in terms of X-ray emission. The detailed mechanism of energy release in flares remains a puzzle, but there is consensus that the energy derives from magnetic fields in active regions, where flares occur, via magnetic reconnection.

Soft X-ray observations from Skylab led to flares being classified as either *compact* or *arcade*-type events. Compact flares occur in small loops, and tend to have rapidly-varying hard X-ray emission, so they are also known as *impulsive flares*. It is unclear as to whether flares really occur in single loops, or always involve multiple loops. Arcade-type flares occur in extended coronal structures with a cusped configuration, and in some the hard X-ray emission is relatively gradual, a class of events known as *gradual flares*. Arcade flares also tend to show a distinctive pattern of two spreading ribbons of $H\alpha$ emission at the chromosphere, and they are often associated with erupting prominences and coronal mass ejections. Figure 9.9 shows a cusped soft X-ray loop in the solar corona, associated with a flare and a CME. Additional flare events are shown in Figure 9.6 above, although often a distinction is retained between flares and X-ray jet events.

Flares produce emission across the electromagnetic spectrum. A variety of emission is produced by accelerated electrons (with energies in the range 10 – 100 keV) that are energised in the corona and precipitate along magnetic field lines to the

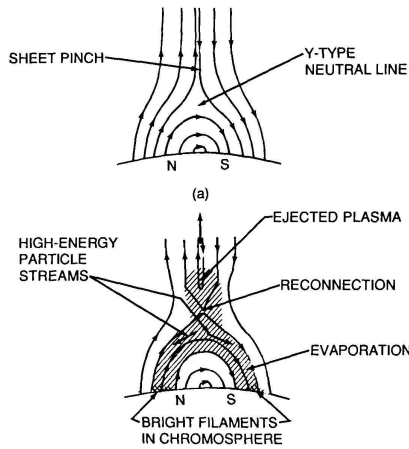


Figure 9.7: The “standard” flare reconnection scenario, according to Sturrock [Tandberg-Hanssen and Emslie, 1988].



Figure 9.8: The ‘Bastille Day 2000’ flare [From <http://www-istp.gsfc.nasa.gov>].

low atmosphere. Observations suggest that a substantial fraction of the flare energy budget resides in these electrons, so the energy release process must involve efficient acceleration of particles. The electrons are *non-thermal*, i.e. have a power-law, rather than Maxwellian, energy spectrum. As the electrons traverse the magnetic field they produce cm and mm wavelength gyrosynchrotron emission, and when they reach the chromosphere they excite atoms to produce $H\alpha$ emission. Hard X-ray emission (i.e. emission at greater than 10 keV) is produced at the footpoints of soft X-ray (1-10 keV) flare loops by *bremstrahlung* when the accelerated electrons collide with ambient ions. Typically double footpoint structures are observed in hard X-ray, although single sources and multiple structures are also seen. Figure 9.10 shows an example of the relative locations of soft and hard X-ray emission in a flare.

The electrons rapidly heat the low atmosphere at loop footpoints, and the heated gas expands up into the loop, a process known as *chromospheric evaporation*. This results in a rise in observed soft X-ray emission during a flare and a temporal correspondence between the integral of hard X-ray light curves and soft X-ray light curves (the *Neupert effect*), as shown in Figure 9.11.

Figure 9.12 shows the hard X-ray light curve of a flare observed by a detector on



Figure 9.9: A cusped soft X-ray loop in the solar corona, observed by the Yohkoh satellite. [From <http://solar.physics.montana.edu/nuggets/1999/>.]

a balloon on 27 June 1980, and Figure 9.13 shows how the hard X-ray spectrum of the flare evolves in time. At first the spectrum is a power law, indicating that the emission is due to non-thermal bremsstrahlung, but later a hot thermal component appears at low energy. This *superhot* component has a temperature of around 10^7 K, and is due to flare-heated material in the corona. Flare loops are much hotter, and also denser ($n \approx 10^{17} \text{ m}^{-3}$) than other coronal loops.

A variety of evidence suggests that the energy release mechanism in flares is fragmentary, involve multiple small-scale energy release events that trigger one another. Large numbers ($\approx 10^4$) of microwave spike bursts are observed in some flares, and they may correspond to individual energy release events. Individual flares may also produce several hundred decimetric type III bursts, each of which corresponds to at least one beam of accelerated electrons propagating in the corona. Figure 9.14 shows observations of decimetric type III bursts produced in a flare. The observed emission from each burst has a frequency that increases with time, corresponding to downwards propagation of a beam in the corona (the emission occurs at the plasma frequency or at a multiple of the plasma frequency). Finally, the frequency-energy distribution of flares estimated from X-ray observations is a power law. A popular explanation for this distribution is in terms of an *avalanche model*, in which the energy release process is highly fragmentary. Obtaining such a model for magnetic reconnection is an area of active research.

9.2.3 Coronal mass ejections

In the early 1970s, coronal mass ejections (then called coronal transients) or CMEs were discovered in satellite observations of the white-light corona. They involve the expulsion of a large amount of material from the corona (up to 2×10^{13} kg) at speeds ranging from $10 - 10^3 \text{ km s}^{-1}$. The mass involved is roughly 10% of the mass of the entire corona, and the associated kinetic energy can be as large as 10^{25} J, comparable to the largest flares.

CMEs apparently involve a large-scale reorganization of the coronal magnetic field. More than half of observed CMEs are associated with erupting filaments (prominences observed on the disk), and many also involve the disruption of a helmet streamer. It is generally believed that CMEs represent a global MHD instability, although there is no accepted theory for the processes involved. CMEs are reproduced in numerous ideal and resistive MHD simulations.

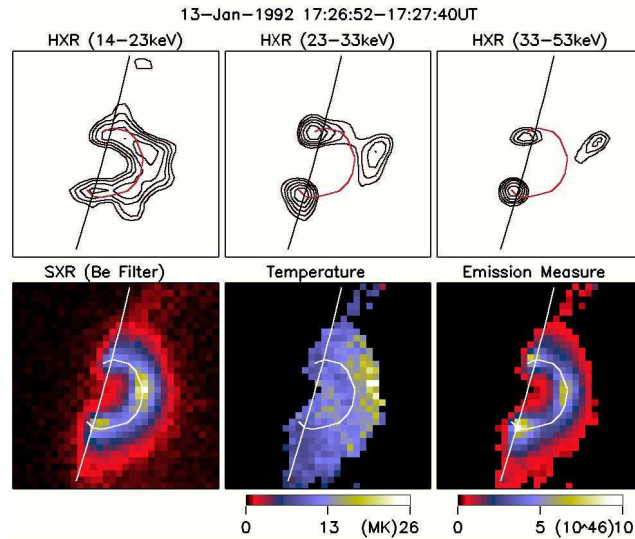


Figure 9.10: Soft and hard X-ray emission in a flare. The top images show hard X-rays at different energies, while the soft X-rays and the inferred temperature and emission measure are shown in the bottom images. Loops are clearly visible in both soft and hard x-rays, with the footpoints clearly illuminated. The source of accelerated particles is believed to be at the top of the loop.

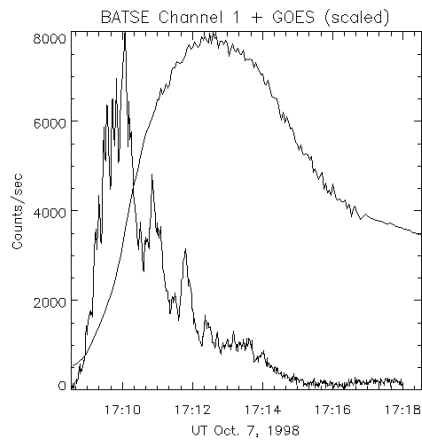


Figure 9.11: The Neupert effect, observed in an impulsive flare. The soft X-ray emission (the smooth curve) appears to be roughly proportional to the time integral of the hard X-ray emission (the spiky curve). [From <http://solar.physics.montana.edu>.]

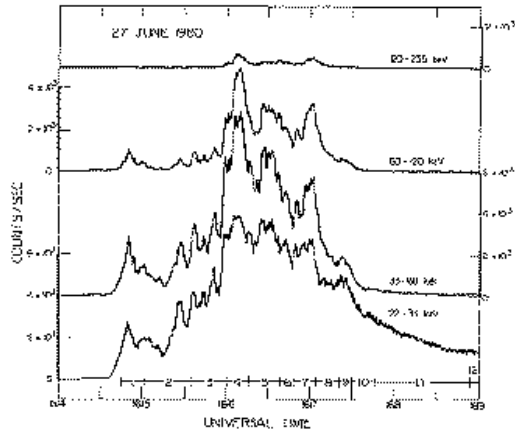


Figure 9.12: Time-history of hard X-ray production in a flare observed on 27 June 1980 [Lin et al., 1981]

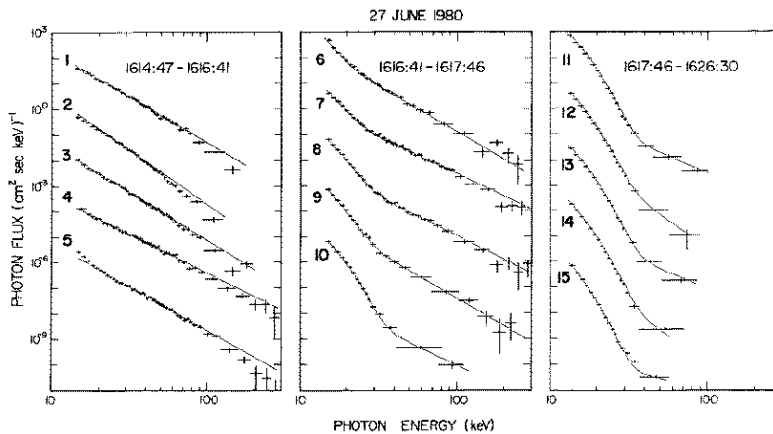


Figure 9.13: Evolution of the hard X-ray spectrum for the 27 June 1980 flare. The numbers correspond to time intervals specified in Figure 9.12 [Lin et al., 1981].]

CMEs were first thought to be caused by flares, but studies have shown that the launch of a CME often precedes a flare (although there may be a weak soft X-ray precursor to the flare which comes before the CME). The detailed relationship between the two phenomena is not well understood. Recently, CMEs have been recognised as having a more direct bearing on solar terrestrial relations than flares. CMEs drive shock waves in the low corona and in the solar wind which accelerate particles. Type II bursts are interpreted as plasma emission from electrons accelerated at CME shocks propagating outwards through the solar corona, and solar energetic particle events (SEPs) – involving particles with energies in excess of 1 MeV at 1 AU – are strongly correlated with CMEs.

9.3 The activity cycle

Regular observations of sunspots have been made since the invention of the telescope, in the 17th century. In 1843 Schwabe was the first to notice that the number of sunspots visible on the Sun does not vary completely randomly but follows a

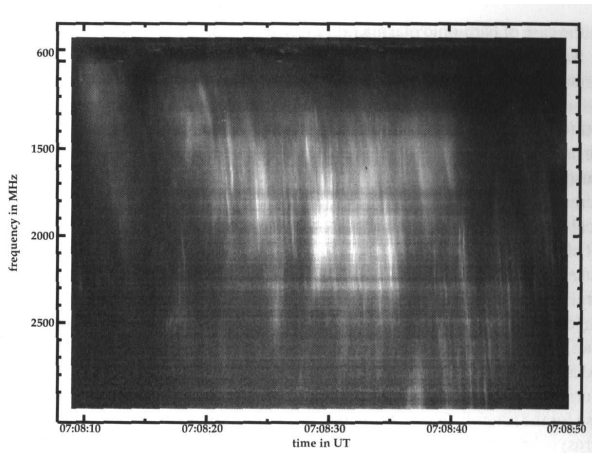


Figure 9.14: Hundreds of decimetric type III bursts produced during a flare [Bastian, Benz and Gary, 1998]

cycle with a period of 11 years, as shown in Figure 9.1. The interval between the times of sunspot maximum varies somewhat, and may be as long as 15 years, or as short as 8 years.

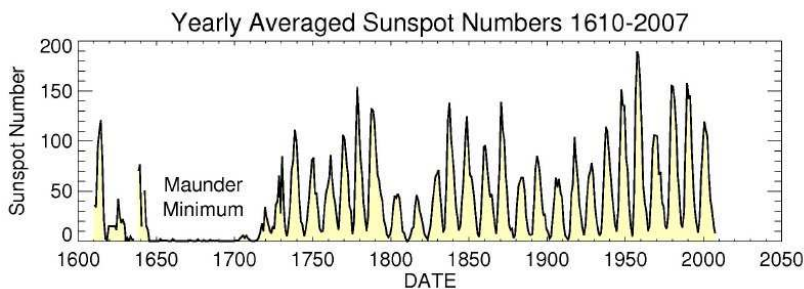


Figure 9.15: The sunspot record. The remarkable low number, or near absence, of sunspots in the late 1600s is known as the *Maunder minimum*. [From <http://science.nasa.gov/>.]

There are also many other patterns in the appearance of magnetic flux at the surface of the Sun, that provide information about the mechanism producing the magnetic field. During a given solar cycle sunspots in one hemisphere tend to have a particular polarity of the field leading and the other polarity following as they rotate across the disk. For example, during Cycle 22 (1987-1997) the leading polarity in the northern hemisphere was generally negative, and the following polarity positive. In the other hemisphere (during the same cycle) the pattern of polarities is reversed. During the next solar cycle, the polarities that are leading and following have interchanged. The phenomenological rule that leading and following polarities alternate with the sunspot cycle is called Hale's law, and it establishes that the underlying periodicity in the generation of the magnetic field is 22 years rather than 11 years.

Another rule is that sunspots tend to appear early in a solar cycle (just after solar minimum) at high latitudes, and then at progressively lower latitudes later in a cycle. At the next cycle, the new-cycle spots are recognisable both because they tend to have a reversed polarity, and because they tend to appear at high latitudes

(whereas the old-cycle spots occupy low latitudes). When a plot of the latitude of emergence versus time is made, a characteristic *butterfly diagram* is produced (Figure 9.16)

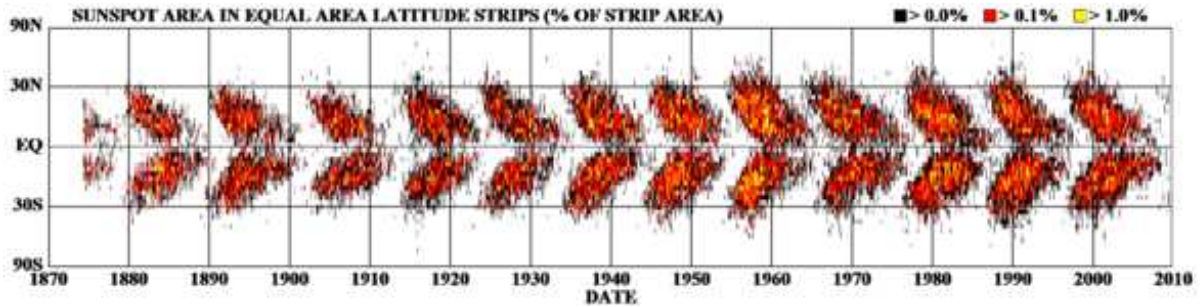


Figure 9.16: A butterfly diagram of the location of sunspots over many solar cycles [From <http://solarscience.msfc.nasa.gov/SunspotCycle.shtml>].

The process behind these patterns, that produces the Sun's magnetic field, is poorly understood. Dynamo models (Lecture 7) attempt to explain the solar cycle in terms of a cyclical regeneration of magnetic field in the convection zone. The models can not, for example, naturally explain the 22-year period. However, there is a strong correlation between subsurface torsional flows seen in helioseismology data and sunspots, as seen in Figure 9.17, that argues strongly for a dynamo model. A detailed theoretical understanding of this does not yet exist.

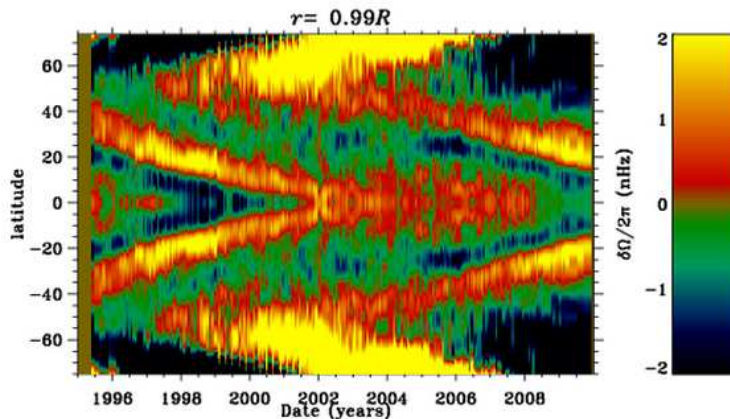


Figure 9.17: Over the course of the solar cycle, bands of slightly faster and slower rotation appear at mid-latitudes and propagate towards the poles and the equator. The similarity to the butterfly diagram for sunspots is striking. [From the GONG website.]

The Sun's magnetic cycle governs solar activity. At solar maximum (sunspot maximum), there are many more solar flares and associated CMEs. The next solar maximum is expected in 2012-2013, after an unusually delayed start to the current cycle.

References

Acknowledgement This lecture is based in part on an earlier lecture by Mike Wheatland, itself based on an outline developed by me.

- Bastian, T.S., Benz, A.O. and Gary, D.E. 1998, *Annual Reviews of Astronomy & Astrophysics*, **36**, 131
- Cravens, J. 1997, *Physics of Solar System Plasmas*, Cambridge.
- Hudson, H. and Ryan, J. 1995, *Annual Reviews of Astronomy & Astrophysics* **33**, 239
- Lin, R., Schwartz, R., Pelling, R. and Hurley, K. 1981, *Astrophysical Journal Letters* **251**, L109
- Oieroset, M., Lin, R.P., Phan, T.D., Larson, D.E., and Bale, S. D. 2002, *Physical Review Letters*, **89**, 195001
- Priest, E., and Forbes, T. 2002, *The Astronomy and Astrophysics Review*, **10**, 313
- Tandberg-Hanssen, E. and Emslie, A.G. 1988, *The Physics of Solar Flares*, Cambridge University Press, Cambridge
- Zweibel, E.G., and Yamada, M. 2009, *Ann. Rev. Astron. Astrophys.* **47**, 291332.